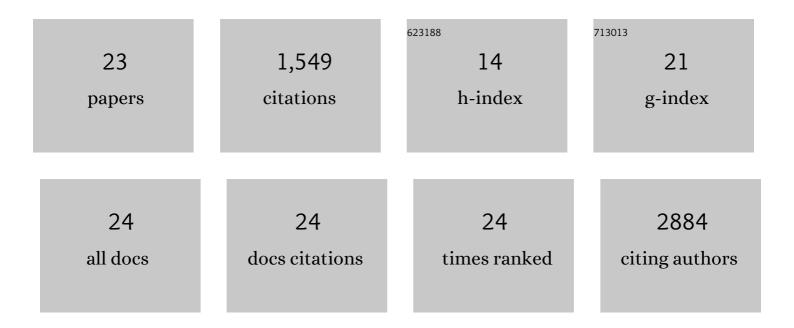
Hunter R Underhill

List of Publications by Year in descending order

Source: https://exaly.com/author-pdf/5931528/publications.pdf Version: 2024-02-01



#	Article	IF	CITATIONS
1	Heterozygous variants that disturb the transcriptional repressor activity of FOXP4 cause a developmental disorder with speech/language delays and multiple congenital abnormalities. Genetics in Medicine, 2021, 23, 534-542.	1.1	17
2	Leveraging the Fragment Length of Circulating Tumour DNA to Improve Molecular Profiling of Solid Tumour Malignancies with Next-Generation Sequencing: A Pathway to Advanced Non-invasive Diagnostics in Precision Oncology?. Molecular Diagnosis and Therapy, 2021, 25, 389-408.	1.6	26
3	Detection of circulating tumor DNA without a tumor-informed search using next-generation sequencing is a prognostic biomarker in pancreatic ductal adenocarcinoma. Neoplasia, 2021, 23, 859-869.	2.3	6
4	Somalier: rapid relatedness estimation for cancer and germline studies using efficient genome sketches. Genome Medicine, 2020, 12, 62.	3.6	48
5	VPS4A Mutations in Humans Cause Syndromic Congenital Dyserythropoietic Anemia due to Cytokinesis and Trafficking Defects. American Journal of Human Genetics, 2020, 107, 1149-1156.	2.6	20
6	The stochastic nature of errors in next-generation sequencing of circulating cell-free DNA. PLoS ONE, 2020, 15, e0229063.	1.1	6
7	VPS4A mutations Cause a Syndrome with Dyserythropoiesis, Hemolytic Anemia, and Neurodevelopmental Delay. Blood, 2019, 134, 339-339.	0.6	Ο
8	Automated size selection for short cell-free DNA fragments enriches for circulating tumor DNA and improves error correction during next generation sequencing. PLoS ONE, 2018, 13, e0197333.	1.1	55
9	DPAGT1 Deficiency with Encephalopathy (DPAGT1-CDG): Clinical and Genetic Description of 11 New Patients. JIMD Reports, 2018, 44, 85-92.	0.7	16
10	A continuousâ€infusion dynamic MRI model at 3.0 Tesla for the serial quantitative evaluation of microvascular proliferation in an animal model of glioblastoma multiforme. Magnetic Resonance in Medicine, 2017, 78, 1824-1838.	1.9	0
11	Pathogenic <i>ASXL1</i> somatic variants in reference databases complicate germline variant interpretation for Bohring-Opitz Syndrome. Human Mutation, 2017, 38, 517-523.	1.1	49
12	Fragment Length of Circulating Tumor DNA. PLoS Genetics, 2016, 12, e1006162.	1.5	502
13	Detecting the effects of Fabry disease in the adult human brain with diffusion tensor imaging and fast boundâ€pool fraction imaging. Journal of Magnetic Resonance Imaging, 2015, 42, 1611-1622.	1.9	7
14	Prediction of High-Risk Plaque Development and Plaque Progression With the Carotid Atherosclerosis Score. JACC: Cardiovascular Imaging, 2014, 7, 366-373.	2.3	59
15	Asymptomatic methylmalonic acidemia in a homozygous <i><scp>MUT</scp></i> mutation (p. <scp>P86L</scp>). Pediatrics International, 2013, 55, e156-8.	0.2	1
16	Fast bound pool fraction imaging of the in vivo rat brain: Association with myelin content and validation in the C6 glioma model. NeuroImage, 2011, 54, 2052-2065.	2.1	118
17	Carotid MRI: a tool for monitoring individual response to cardiovascular therapy?. Expert Review of Cardiovascular Therapy, 2011, 9, 63-80.	0.6	17
18	A combined solenoidâ€surface RF coil for highâ€resolution wholeâ€brain rat imaging on a 3.0 tesla clinical MR scanner. Magnetic Resonance in Medicine. 2010. 64. 883-892.	1.9	7

HUNTER R UNDERHILL

#	Article	IF	CITATIONS
19	MRI of carotid atherosclerosis: clinical implications and future directions. Nature Reviews Cardiology, 2010, 7, 165-173.	6.1	143
20	Direct quantitative comparison between cross-relaxation imaging and diffusion tensor imaging of the human brain at 3.0ÅT. Neurolmage, 2009, 47, 1568-1578.	2.1	53
21	Effect of rosuvastatin therapy on carotid plaque morphology and composition in moderately hypercholesterolemic patients: A high-resolution magnetic resonance imaging trial. American Heart Journal, 2008, 155, 584.e1-584.e8.	1.2	223
22	Carotid Plaque Morphology and Composition: Initial Comparison between 1.5- and 3.0-T Magnetic Field Strengths. Radiology, 2008, 248, 550-560.	3.6	103
23	Automated measurement of mean wall thickness in the common carotid artery by MRI: A comparison to intima-media thickness by B-mode ultrasound. Journal of Magnetic Resonance Imaging, 2006, 24, 379-387.	1.9	71